VUV spectroscopy and photo-processing of astrochemical ices: an experimental study

Nigel J. Mason,*[a] Anita Dawes,[a] Philip D. Holtom,[a] Robin J. Mukerji,[a] Michael P. Davis,[a] Bhalamurugan Sivaraman,[a] Ralf I. Kaiser,[b] Søren V. Hoffmann[c] and David A. Shaw[d]

Received 21st December 2005, Accepted 13th February 2006
First published as an Advance Article on the web 12th May 2006
DOI: 10.1039/b518088k

In order to understand much of the chemistry that underpins astronomical phenomena (*e.g.* star and planet formation) it is essential to probe the physico-chemistry of ice surfaces under astronomical conditions. The physical properties and chemical reactivity of such icy surfaces depends upon its morphology. Thus it is necessary to explore how the morphology of astrochemical ices is influenced by their local environment (*e.g.* temperature and pressure) and the mechanisms by which they are processed. In this paper we report the results of a series of experiments to explore the morphology of a variety of molecular ices using VUV spectroscopy. Spectral signatures are found that may allow the morphology of such ices to be identified.

Introduction

An understanding of the chemical evolution of the universe necessarily requires that we gain a detailed knowledge of the complex chemistry occurring in both the present and past history of the universe. Such 'astrochemistry' has several distinct differences from that occurring in the terrestrial and industrial environments with which most of our chemical studies are concerned; for example:

(i) Due to the low densities encountered in many astronomical regions the chemical time scales may be tens of thousands (or even millions) of years, with simple binary molecular encounters being predominant in the gaseous phase.

(ii) The chemistry may occur at much lower temperatures than those commonly encountered on Earth, *e.g.* at temperatures as low as a few Kelvin in the interstellar medium thus emphasizing so-called 'barrierless' chemical reactions.

(iii) Chemical species not commonly found on Earth may play a key role in astrochemistry *e.g.* the molecular ions H_3^+ and HeH^+ both of which are believed to have played a key role in the first chemical reactions to have ever occurred in the history of the universe.

Obtaining information on the different chemical environments within our universe has relied critically upon the continuing technological advances in observational astronomy and computer modelling combined with a growing experimental programme that seeks to reproduce such conditions in the laboratory. Hence it has only been in the last two to three decades that our knowledge of the major chemical processes underpinning the chemical evolution in the Universe has developed sufficiently that we may now, with some confidence, propose reasonable hypotheses to describe some of the observational data and explore how chemistry affects star/planet formation

[a] *Department of Physics and Astronomy, The Open University, Milton Keynes UK MK7 6AA*
[b] *Department of Chemistry, University of Hawaii at Manoa, Honolulu, Hawaii, 96822, USA*
[c] *Institute for Storage Ring Facilities, Department of Physics and Astronomy, University of Aarhus, DK-8000, Aarhus C, Denmark*
[d] *Synchrotron Radiation Department, CCLRC Daresbury Laboratory, Keckwick Lane, Warrington, Cheshire, UK WA4 4AD*

Table 1 Inventory of ices in space normalized to water (100)[37]

Species	Elias 16	NGC 7538 IRS 9	GL 7009S	W33A	GL 2136	Sgr A	Comets
H_2O	100	100	100	100	100	100	100
CO (total)	25	16	15	8	2	<12	5–30
CO (polar)	3	2	—	6	2		
CO (nonpolar)	22	14	—	2	—	—	—
CO_2 (total)	18	22	21	13	16	14	3–20
CO_2 (polar)	18	14	—	11	13	14	—
CO_2 (nonpolar)	<1	8	—	2	3	<1	—
CH_4		2	4	1.5		2	1
CH_3OH	<3	5	30	18	6	<4	0.3–5
H_2CO		4	3	6	3	<3	0.2–1
HCOOH		3		7	—	3	0.05
OCS	<0.2	—	0.2	0.2	—	—	0.5
NH_3	≤9	13		15	—	20–30	0.1–1.8
XCN	<0.5	1	1.5	3.5	0.3		0.01–0.4

and postulate the role of astrochemistry in the formation of molecules essential to the emergence of life—the latter being a core part of the new scientific discipline of 'astrobiology' upon which much of the ESA and NASA space programmes will be focused in the 21st century.

In this article we discuss the role of chemistry within 'ices'† found within the universe and in particular emphasize that in understanding such chemistry it is essential to understand the role of ice morphology if we are to unravel the complex chemistry leading to molecular formation in/on such ices and the physical properties of icy bodies in the universe.

Ices are found in most regions of the universe (Table 1) due to the inherent temperature of most of the universe being well below that required for most molecules to 'freeze' out onto any suitable surface. Thus most planetary and lunar surfaces in our own solar system (Venus and Mercury being the exceptions) contain large amounts of ice. Some 10% of the Earth's surface is today covered by ice while Mars has permanent polar ice caps composed mostly of solid carbon dioxide and recent data from both the ESA Mars Express missions and NASA Mars Odyssey suggest the possibility of large deposits of subsurface ice (probably in the form of water).[1–3] Most of the outer solar system bodies are covered with ices, predominantly water-ice, although more volatile species may be present on Triton and Pluto under very low temperature conditions (*i.e.* < 60 K).[4] A number of the satellites of Jupiter and Saturn are ice covered. In particular, Europa has been studied in detail to establish whether it is possible for a subsurface ocean to be present[5] and recent evidence for the presence of ozone (previously thought to be characteristic of bioactivity) has been reported on Saturn's moons Rhea, Dione[6] and Enceladus and the Jovian moon Ganymede.[6,7] Nor should we forget the large number of Kuiper belt objects located beyond Neptune and cometary systems which are mainly comprised of ice.[8] Hence perhaps ice is the most common phase of matter in our own solar system.

Beyond our solar system in those vast regions of the interstellar medium (ISM), themselves the 'chemical factories' for over the 150 molecules now observed by astronomical observations, it is now apparent that much of the chemistry arises from heterogeneous chemistry on icy surfaces of dust grains. Dust grains are produced by stars which have evolved off the main sequence. The silicate particles form in the atmospheres of cool stars, and carbon grains in the atmospheres of cool carbon stars. These grains are released when supernovae/novae cause the ejection of stellar material into space forming dust clouds.[9] Once in the ISM the grains cool (new grains may also form). When the grains have cooled down to about 15 K, they form the cores for the growth of ice mantles. The mantles are formed by accretion of (gas phase) molecules and by surface reactions between atoms of oxygen, carbon, nitrogen, sulfur, along with atomic hydrogen which may subsequently form H_2. Indeed the formation of molecular hydrogen, the most abundant molecule in the universe, can only be described by the recombination of H atoms on cold dust surfaces in such regions.

† Astronomers use the term 'ice' to refer to any solid material frozen out from their volatile gas counterparts.

These ice mantles then act as chemical 'factories' with surface (heterogeneous) chemistry allowing more complex molecules to form *e.g.* H_2O, H_2S, CH_3OH, OCS, OCN . . . In addition these mantle ices are always being processed by ultraviolet radiation, cosmic rays or stellar winds. This processing changes the basic composition of the ices and causes some complex organic refractory residues to form. Eventually the cloud may become a denser molecular cloud. It is in these denser clouds that organic mantles are formed, layering the core like the rings in a tree trunk. Once a critical density is reached *star formation* begins.

These dense clouds collapse under their own gravity, to form protostars surrounded by a protostellar disk, from which stars, planets and small bodies form, within an evolutionary period of $\sim 10^{6-8}$ years.[9] The interstellar dust and gas are processed according to their proximity to the star, thermal desorption evaporating the ices close to the star while further out in the protostellar disk volatile species may recondense, forming a 'new generation' of icy grains with different chemical composition and morphology to those in the original dense cloud.

Protoplanetary systems may then be formed in the protostellar disk around newly formed low mass stars. However, how planet formation overcomes the counter effect of the stellar wind (literally 'blowing it' away) remains unclear. Recent experiments studying the physical properties of ice mimics in these protoplanetary disks may provide a valuable clue. The ice encountered there (at temperatures 5–15 K) has a different morphology which leads to a significantly different sticking coefficient such that when it collides with another ice mantle it acts like 'glue'. The ice spontaneously becomes electrically polarized with the electrical forces able to 'stick' the icy grains together.[10]

Thus in order to understand much of the chemistry that underpins larger astronomical phenomena (*e.g.* star and planet formation) it is essential to probe the physico-chemistry of ice surfaces under astronomical conditions. The physical properties and chemical reactivity of the ice will depend crucially upon the morphology of the ice surface and thus it is necessary to explore how the morphology of astrochemical ices is influenced by their local environment (*e.g.* temperature and pressure) and the mechanism by which these are processed.

Ices can exist in a number of different forms the most common being crystalline and amorphous. Crystalline ices are typically formed at higher temperatures and are most common in terrestrial environments. Amorphous ices are commonly formed at low temperatures (<130 K) and resemble liquids, in that they have no long-range molecular order. In this paper we report the results of a series of experiments to explore the morphology of a variety of molecular ices using VUV spectroscopy. Several spectral signatures are found that may allow the morphology of such ices to be identified.

Experimental

Reproducing the conditions under which astrochemistry occurs in the interstellar medium or on a planetary surface places several constraints on the laboratory simulations. In particular it is necessary to:

(i) Create the vacuum conditions suitable for the deposition of gases to form an astrochemical ice mimic.

(ii) Provide cryogenic cooling to create and maintain ice at temperatures typical of the icy body being mimicked.

(iii) Provide suitable sources to mimic the processing of the ice comparable with those found in the astrochemical environment.

We have designed a laboratory apparatus (Fig. 1) that is suitable for creating icy films that are a good representation of those in the astrochemical environment. The apparatus comprises of an ultra high vacuum chamber capable of routinely attaining pressures in the 10^{-10} mbar range with the residual gases being mainly hydrogen—as is common in the ISM. The vacuum chamber is fitted with a continuous flow liquid helium cryostat (AS Scientific) capable of reaching a base temperature of approximately 15 K. At the end of the cryostat we attach a magnesium fluoride (MgF_2) or calcium fluoride (CaF_2) substrate (ϕ 20 mm $\times$ 2 mm) which allows high efficiency transmission of ultraviolet light.

Ice films are grown *in situ* by direct vapour deposition onto the liquid helium cooled substrate. Deposition is carried out at normal incidence *via* a 3 mm nozzle directed onto the substrate which is 18 mm from the exit of the nozzle. Temperature control of the sample is achieved using an ITC503

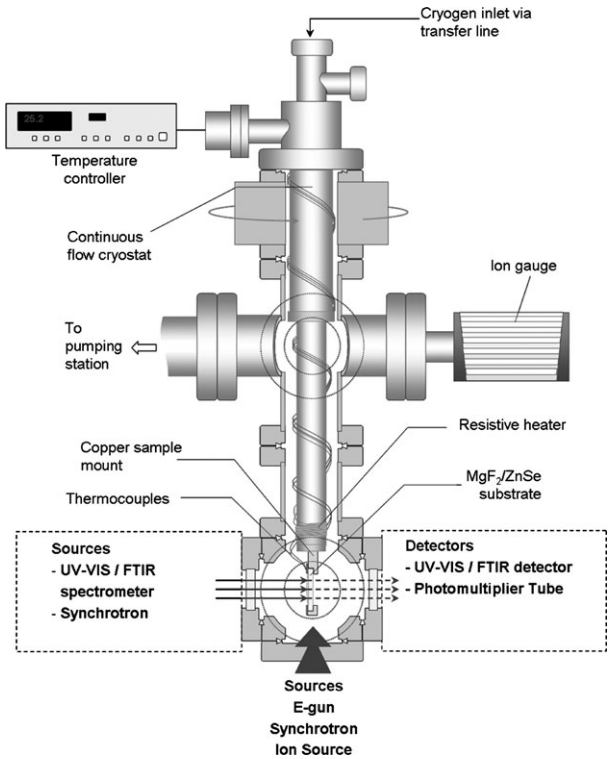

Fig. 1 Schematic of the apparatus used to measure VUV spectra of astrochemical ices.

Oxford Instruments temperature controller, with the ice temperature being continually monitored using *N*-type and gold-iron/Chromel thermocouples situated close to the sample.

In order to determine the sample thickness in our experiments we adopted a laser interference technique. The reflected signal from a He–Ne laser directed onto the ice film was measured using a photodiode as the gas is deposited onto the substrate. A sinusoidal interference pattern is created from the interference between the light reflected from the ice surface and the substrate. This pattern was measured as an increasingly thick layer of ice is deposited allowing us to profile the thickness of the ice using eqn (1), where d is the ice thickness, λ_0 is the He–Ne wavelength, n_1 is the refractive index of the ice (estimated from the ratio between the maximum and minimum reflected intensity of the light[11]) and θ_1 is the angle of the laser within the ice.

$$d = \frac{\lambda_0}{2n_1 \cos\theta_1} \tag{1}$$

In our research programme we are utilising a variety of different tools to process the ice. These include: thermal processing using the ITC503 Oxford Instruments temperature controller, ion implantation using the Electron Cyclotron Resonance (ECR) ion sources at Queens University Belfast; electron irradiation using an electron gun placed directly into the chamber and UV processing using a high intensity UV lamp and synchrotron radiation.

In this paper we report results using synchrotron radiation to measure the VUV spectroscopy of deposited ice films as a probe of the ice morphology under thermal processing. Results have been recorded at two synchrotron facilities: ASTRID at the University of Aarhus, using the UV1 monochromator beamline and beamline 3.1 at the UK Daresbury Synchrotron Radiation Source.

Spectra were acquired before and after deposition to obtain the incident (I_0) and transmitted (I_t) intensities from which absorbance spectra are calculated. Photo-absorption cross sections (σ/cm^2) were calculated for samples deposited under the same conditions for which sample thickness

measurements were made. The Beer–Lambert law is used to calculate the cross sections as a function of photon energy:

$$I_t(\lambda) = I_0(\lambda)e^{-nl\sigma(\lambda)} \quad (2)$$

where n is the number density in cm^{-3} and l is the path length (ice thickness) in cm. It is not directly possible to determine the cross sections accurately for any of the processed samples due to changes in the properties of the solid film, after irradiation, changes which affect the structure and the optical properties of the ice.

VUV absorption spectra were recorded in transmission mode using a photomultiplier tube (PMT) to record the intensity of the transmitted light at 0.1–0.2 nm resolution intervals. The incident wavelength from the synchrotron was selected using a diffraction grating and spectra were acquired over the range 120 to 320 nm (10.33 to 3.87 eV). At both facilities the minimum wavelength was determined by the materials used for the entrance and exit windows of the vacuum chamber. For the spectra presented in this paper, a lithium fluoride (LiF) entrance window and MgF_2 or CaF_2 substrate were used at both beamlines. Thus the minimum wavelength at which reliable data could be acquired was 10.33 eV (120 nm) and 9.92 eV (125 nm) respectively. At the UV1 beamline a VUV sensitive PMT was used with a MgF_2 exit window and the interspace between the window and the PMT was flushed with helium at shorter wavelengths to eliminate absorption due to atmospheric O_2. At beamline 3.1 a PMT sensitive to visible wavelengths was used with a glass exit window coated in sodium salicylate, which converts UV photons to visible.

All gases used in these experiments were commercially available with a quoted purity of more than 99.9%. Water samples were drawn from distilled water that was freeze–pump–thawed and degassed under vacuum.

Results: VUV spectroscopy of astrochemical ices

Case study 1: water

Water ices appear to be ubiquitous in space and are by far the most abundant condensed-phase species in our universe. It is not however clear which type of ice provides the best mimic for water on the surface of dust grains in the ISM or on a planetary or lunar surface. Water is perhaps the most complex ice yet studied existing in 17 different 'phases' both crystalline and amorphous (Fig. 2 and Table 2). All the crystalline phases of ice involve the water molecules being hydrogen bonded to four neighbouring water molecules. In all cases the two hydrogen atoms are equivalent, with the water molecules retaining their symmetry, and they all obey the 'ice' rules: two hydrogen atoms near each oxygen, one hydrogen atom on each O···O bond. The H–O–H angle in the ice phases is expected to be a little less than the tetrahedral angle (109.47°), at about 107°.

Water ice as most commonly encountered on Earth as snow is hexagonal ice (ice I_h). When subjected to higher pressures or varying temperatures, water ice can form a dozen different 'phases' including a cubic structure ice (I_c) but cooling I_h causes a different arrangement to form in which the protons move, XI. With both cooling and pressure more types exist, each being created depending on the phase diagram of ice (Fig. 2). These are types II, III, V, VI, VII, VIII, IX, and X all of which can be maintained at ambient pressure. The types are differentiated by their crystalline structure, ordering and density. There are also two metastable phases of ice under pressure, both fully hydrogen disordered, these are IV and XII. As well as crystalline forms solid water can exist in amorphous states, marked by disordered structure. High pressure forms of amorphous ice are low density amorphous ice (LDA), high density amorphous ice (HDA), very high density amorphous ice (VHDA) and hyperquenched glassy water (HGW). Amorphous solid water (ASW) is formed in the laboratory by vapour deposition onto a cold substrate (<130 K) at low pressures. This form of ice, which resembles HDA is believed to be the closest mimic to interstellar ices. The structure of this type of ice is highly porous[12] and provides a vast surface area for heterogeneous processes as well as pores for trapping volatile species.[13]

We have recorded VUV transmission spectra of water ice deposited at 25 K (Fig. 3). Under such conditions the water ice deposited on the CaF_2 substrate is expected to be amorphous (ASW). This spectrum should be compared with that of gaseous water. In many astrochemical models gaseous spectra are used to determine photo-absorption cross sections in the molecular clouds and the

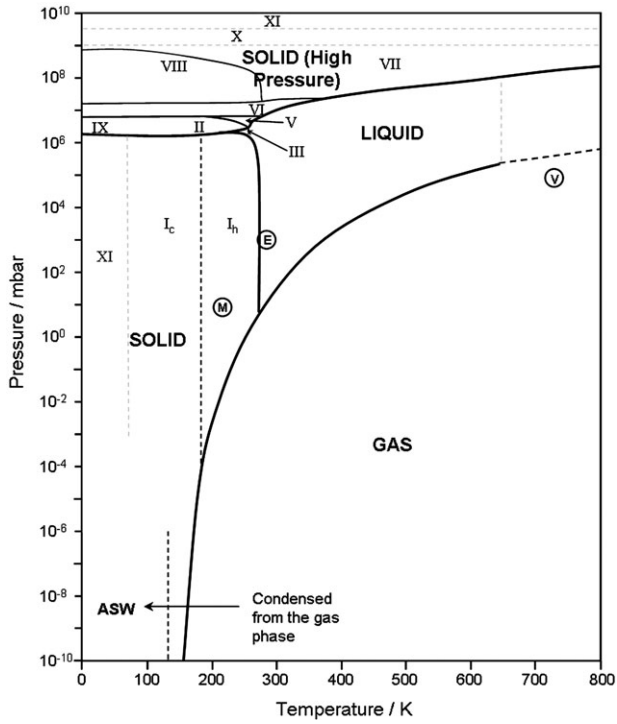

Fig. 2 Phase diagram of water showing the conditions for the formation of the different phases of water. The mean surface conditions on Earth (E), Mars (M) and Venus (V) are indicated.

products due to photolysis, this is recognized as being unsatisfactory, but in the absence of data on ice films, was necessary. The present data show that such an assumption may lead to considerable errors with many features observed in the gaseous phase not being observable in the solid phase. Water is a good example to illustrate such differences.

Table 2 Different structures of different forms of water ice adapted from http://www.lsbu.ac.uk/water

Type of water ice	Density/g cm^{-3}	Structure	Dielectric constant, ε_S
Hexagonal ice, I_h	0.92	Hexagonal	97.5
Cubic ice, I_c	0.92	Cubic	
ASW	0.94–0.1612	Amorphous	
LDA	0.94	Amorphous	
HDA	1.17	Amorphous	
VHDA	1.25	Amorphous	
Ice II	1.17	Rhombohedral	3.66
Ice III	1.14	Tetragonal	117
Ice IV	1.27	Rhombohedral	
Ice V	1.23	Monoclinic	144
Ice VI	1.31	Tetragonal	193
Ice VII	1.50	Cubic	150
Ice VIII	1.46	Tetragonal	4
Ice IX	1.16	Tetragonal	3.74
Ice X	2.51	Cubic	
Ice XI	0.92	Orthorhombic	
Ice XI	>2.51	Hexagonal	
Ice XII	1.29	Tetragonal	

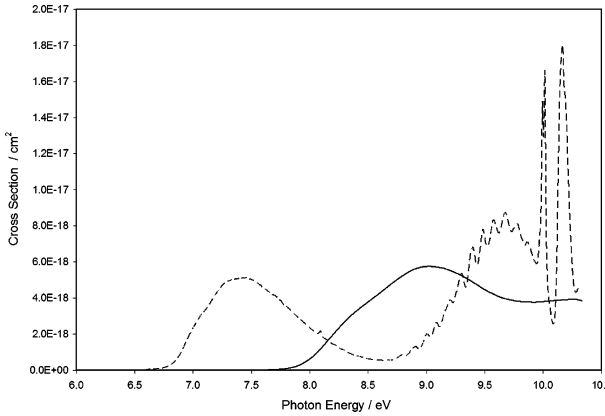

Fig. 3 Comparison of VUV photo-absorption spectrum of condensed water (solid line) at 25 K adsorbed onto CaF_2 substrate with the gas phase spectrum (dashed line) at 295 K.

Three absorption bands centred at 7.447, 9.672 and 10.011 eV have been identified in the gaseous spectrum as transitions from the $\tilde{X}^1A_1$ lowest neutral ground state to the $\tilde{A}^1B_1$, $\tilde{B}^1A_1$ and $\tilde{C}^1B_1$, respectively; a fourth band at 10.163 eV has been identified as $\tilde{D}^1A_1 \leftarrow \tilde{X}^1A_1$. The first band is quite broad and diffuse structure is observed while the other bands are rich in structure with their peak positions and assignments being recently reported in some detail.[14]

The excitation in the 6.5–9.0 eV energy region corresponds to the first absorption band $4a_1{:}\tilde{A}^1B_1 \leftarrow {}^1b_1{:}\tilde{X}^1A_1$ of H_2O; the absorption is mainly a continuum, peaking at 7.447 eV (5.184 Mb). The remarkable behaviour of this transition is its dissociative character into $OH(\tilde{X}^2\Pi) + H(^2S)$ upon photo-excitation. In the energy range 8.5–10 eV the features observed correspond to $3sa_1{:}\tilde{B}^1A_1 \leftarrow 3a_1{:}\tilde{X}^1A_1$ and $3sa_1{:}\tilde{C}^1A_1 \leftarrow {}^1b_1{:}\tilde{X}^1A_1$ transitions. This band is also mainly dissociative upon photo-excitation to $OH(\tilde{A}^2\Sigma^+) + H(^2S)$. For the valence 9.9–10.8 eV energy region, excitation is attributed to $nsa_1/4a_1{:}\tilde{C}^1A_1 \leftarrow 1b_1{:}\tilde{X}^1A_1$ and $npa_1/npb_1\tilde{C}^1A_1 \leftarrow 1b_1{:}\tilde{X}^1A_1$ transitions.[14] This energy band is characterised by sharp peaks superimposed on a relative low background. The $\tilde{C}$ state is bonding in the H–OH coordinate. However, at sufficiently large HOH angles and H–OH distances (<1.6 Å), a water molecule in its linear configuration can reach the $\tilde{A}1B_1$ state *via* a linear Renner–Teller intersection. Since the $\tilde{A}$ state is strongly antibonding correlating with $OH(\tilde{X}^2\Pi) + H(^2S)$, the direct transition $\tilde{B}^1A_1 \leftarrow \tilde{X}^1A_1$ is also possible *via* a conical intersection at these H–OH bond distances. Therefore, these processes are dominant and OH is left in its electronic ground state.

The spectrum of condensed phase water is significantly different. The peak of the lowest absorption band $4a_1{:}\tilde{A}^1B_1 \leftarrow 1b_1{:}\tilde{X}^1A_1$ is blue shifted from 7.45 eV (167 nm) to 8.61 eV (144 nm) while there is a complete absence of vibrational structure at higher energies. The lowering in the excitation energy[15,16] of the electronic state is common upon transfer from the gaseous to solid phase suggesting that photolysis and hence photo-dissociation of molecules occurs at a higher energy (shorter wavelengths) in a solid phase in turn ensuring that photo-chemistry in an ice film requires higher energy photons (or electrons).

The absence of fine structure is commonly due to the absence of Rydberg series in the solid phase since such states (with their larger orbital size) often can not propagate in the solid phase. However the presence or absence of vibrational structure within valence states may also provide a clue as to the morphology of the ice, with sulfur dioxide being a good example (see below).

Case study 2: carbon monoxide

Carbon monoxide is a simple linear molecule, a common substance found on earth and in space. For instance Federman *et al.*[17] report the ultraviolet signature of CO towards ρ Oph A and χ Oph recorded using the Goddard High Resolution Spectrograph on the Hubble Space Telescope. After H_2, CO is the most abundant molecule in the ISM.[18] The rotational lines of CO are often widely

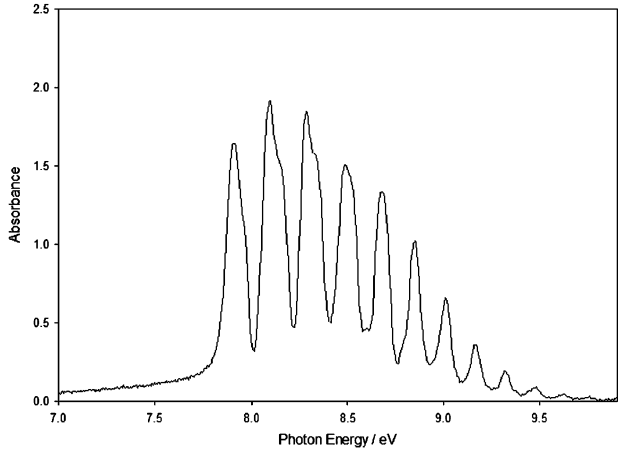

Fig. 4 VUV transmission spectrum of solid CO at 20 K between 7 and 10 eV.

used as a tracer of molecular material in interstellar clouds. The CO "Fourth Positive Band system" ($A^1\Pi - X^1\Sigma^+$) has also been observed in the Sun, several planets and the ISM. The air glow spectrum of Mars and Venus shows evidence of these emissions from the impact of photoelectrons and the effects of solar UV photons.[19] In the solid phase, the fundamental stretching mode of CO in the infrared spectrum is highly sensitive to the environment in which it resides[20,21] and it has therefore been used as an important marker in determining the nature of the ices on dust grains in the ISM.

The VUV spectrum of CO deposited onto a CaF_2 substrate at 20 K exhibits a strong vibrational progression (Fig. 4). We identify the transition as the ($\tilde{A}^1\Pi \leftarrow \tilde{X}^1\Sigma^+$) transition and have compared our work to previous results[22] on solid CO (Table 3). There is also evidence of splitting in some of the peaks, shown in parenthesis in Table 3.

We observe a vibrational progression containing 12 bands identified as (0,0) to (11,0) we do not see the (12,0) transition observed by Brith and Schnepp[22] due to our low sensitivity in the high energy region. The (0,0) transition is shifted by 0.31 eV from the gas phase with the shift becoming

Table 3 Vibrational assignments in the VUV spectrum of pure solid CO at 20 K; numbers in parenthesis indicate band splitting

ν'	Solid phase energy/eV	Solid phase energy from Brith and Schnepp[22]/eV	Gas phase energy/eV	ΔE (gas − solid)
11	9.78	9.77	9.95	0.18
10	9.62	9.63	9.81	0.18
9	9.48	9.48	9.67	0.19
8	9.31	9.33	9.53	0.20
7	9.16	9.18	9.38	0.20
6	9.01	9.02	9.22	0.20
5	8.88	8.86	9.07	0.21
4	8.68	8.69	8.90	0.21
3	8.48	8.49	8.74	0.26
	(8.51)	(8.54)		
2	8.29	8.29	8.57	0.28
	(8.33)	(8.35)		
1	8.09	8.10	8.39	0.30
	(8.14)	(8.17)		
0	7.90	7.91	8.21	0.31
	(7.96)	(7.97)		

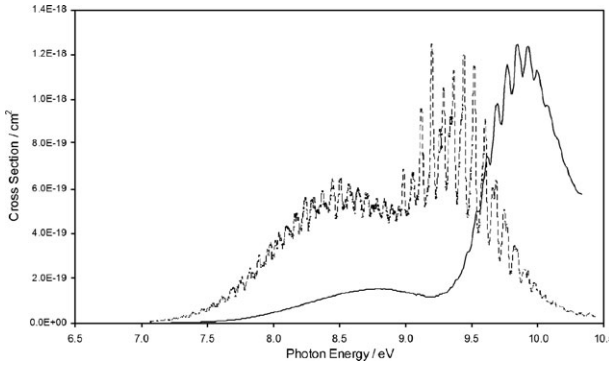

Fig. 5 VUV transmission spectrum of solid (solid line) and gaseous CO_2 (dashed line) from Yoshino *et al.*[25] between 6.5 and 10.5 eV.

smaller until the (4,0) transition whereafter the shift remains approximately constant (0.18–0.21 eV). The (0,0) to (3,0) bands of CO exhibit a crystal field splitting identified as Davydov splitting.[22] Davydov splitting is defined as "*the splitting of bands in the electronic or vibrational spectra of crystals due to the presence of more than one (interacting) equivalent molecular entity in the unit cell*". Evidence of Davydov splitting may have some important consequences in astrochemical studies since it provides both a new spectral signature for the ice morphology and widens the wavelength region over which UV light may be absorbed in the ice. This is clear in pure SO_2 ice where Davydov splitting leads to UV extinction in a previously transparent part of the UV spectrum (see case study 5).

Case study 3: carbon dioxide

Carbon dioxide is the second most abundant molecular ice in the universe existing in two forms: polar and non polar, the former being formed from a water–CO_2 complex. Although there have been several IR studies of CO_2 ices under astronomical condition studies of the electronic state spectroscopy of CO_2 are rare.[23,24] We have recorded the spectrum of solid CO_2 between 120 nm (10.33 eV) and 180 nm (6.89 eV) shown in Fig. 5, compared with the gas phase data of Yoshino *et al.*[25] The VUV transmission spectrum shows two broad bands centred about 8.8 and 9.9 eV that are assigned to the $^1\Delta_u \leftarrow {}^1\Sigma_g^+$ and $^1\Pi_g \leftarrow {}^1\Sigma_g^+$ transitions respectively. The higher energy transition exhibits extensive vibrational structure with a mean separation of 0.076 ± 0.003 eV (609.24 cm^{-1}) which are in good agreement with the only previous data of Monahan and Walker[24] (Table 4), although we have also found evidence for several weaker features at lower energies.

Table 4 Positions of vibrational bands in the pure CO_2 ice spectrum at 20 K

This work		Monahan and Walker[24]	
E/eV	ΔE/eV	E/eV	ΔE/eV
10.22			
10.14	0.07		
10.07	0.07		
10.00	0.07		
9.93	0.07	9.90	
9.85	0.08	9.82	0.08
9.77	0.08	9.74	0.08
9.70	0.07	9.67	0.07
9.62	0.08	9.59	0.08
9.54	0.08	9.53	0.06
9.47	0.07		
9.39	0.08		

The lower lying transition $^1\Delta_u \leftarrow {}^1\Sigma_g^+$ arises due to the promotion of an electron from the $1\pi_g$ orbital to the first unoccupied $2\pi_u^*$ orbital. Once again the solid phase spectrum is blueshifted by some 0.3 eV compared to the gaseous phase, although this is less than in water since CO_2 is not able to hydrogen bond. The observed $^1\Pi_g \leftarrow {}^1\Sigma_g^+$ transition arises as a result of the promotion of a $1\pi_g$ electron to the $3s\sigma_g$ orbital. This state is reported to have Rydberg or Rydberg-valence character[23] which may explain the differences observed in the shape of the peak compared to its gas phase equivalent with the valence-like features being more strongly enhanced than the Rydberg in the solid phase. Furthermore there is a relatively larger shift (0.6 eV) in energy of the $^1\Pi_g \leftarrow {}^1\Sigma_g^+$ transition which is attributed to a greater perturbation of the Rydberg orbital in the solid than the valence orbital in the $^1\Delta_u \leftarrow {}^1\Sigma_g^+$ transition.

This partial separation of valence and Rydberg like characteristics is another feature of solid ice films and once again highlights the dangers in using gas phase data to mimic ice photolysis.

Case study 4: oxygen and nitrogen

Both oxygen and nitrogen are believed to be abundant constituents of interstellar grain mantles.[26,27] However, being homonuclear diatomics, their direct identification is not possible as their fundamental vibrations are infrared inactive. Although in the solid phase interactions with neighbouring molecules may alter the symmetry of the molecules slightly allowing their fundamental transitions to be weakly infrared active. It is unlikely that such spectra can be easily observed in any remote astronomical measurements. In contrast, VUV spectroscopy may be a useful tool in the laboratory to study the morphology of N_2 and O_2 ices and their interaction with other molecules in ice mixtures.

Fig. 6 and 7 show preliminary spectra of solid O_2 and N_2 respectively, each compared with the corresponding gas phase. The spectra are shown on the absorbance scale as calibration thickness measurements for these solids have not yet been made. It is clear in both cases that new bands appear in the spectra that were not present in the gas phase.

The broad continuum between 7.0 and 9.8 eV in the gas phase O_2 spectrum is the transition $\tilde{B}^3\Sigma_u^- \leftarrow \tilde{X}^3\Sigma_g^-$ from the ground state and is known as the Schumann–Runge band. Again there is an apparent blue shift from the gas phase to the solid phase (Fig. 6). A new band, peaking at 7.0 eV is also visible. At this stage it is not possible to assign this band, but one possibility is that it is a signature of oxygen dimer $(O_2)_2$.

Solid N_2 exhibits vibrational structure between 8.4 and 10.8 eV (Fig. 7) or possibly higher (the range limited by the high energy cut off). The spectrum shows two vibrational progressions $a^1\Pi_g \leftarrow \tilde{X}^1\Sigma^+$ and $w^1\Delta_u \leftarrow \tilde{X}^1\Sigma_g^+$ both of which are electrically dipole forbidden in the gas phase. Observation of forbidden transitions is another characteristic of solid phase spectra arising due to breakdown of selection rules in the solid matrix as the symmetry of the molecules is perturbed. The

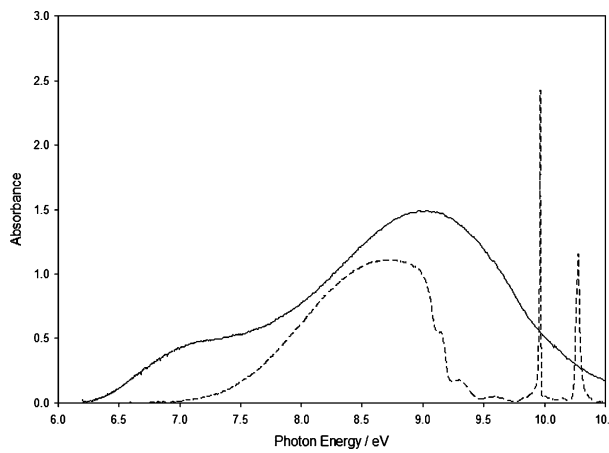

Fig. 6 VUV spectra of solid (solid line) and gaseous (dashed line) O_2.

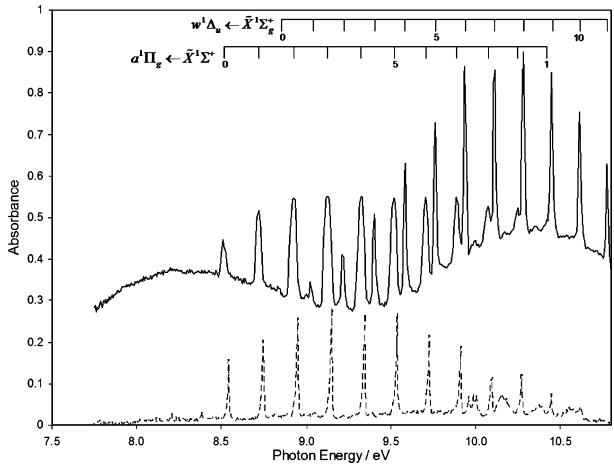

Fig. 7 VUV spectra of solid (solid line) and high pressure gaseous (dashed line) N_2. Spectra are displaced for clarity.

intensity of the bands is very weak and a very thick sample needed to be deposited ($\sim 20 \times$ that of CO) to clearly observe them. Table 5 shows the positions of the vibrational bands for both solid and gas phase spectra. These are in good agreement with Boursey *et al.*[28] Two broad continua are visible in the N_2 spectrum between 7.5 and 9.3 eV and 9.3 and 11 eV. At this stage it is not possible to ascertain what the origins of these bands are although the dimer is again possible. Further study is in progress to investigate the spectra of both solid N_2 and O_2 in more detail.

Case study 5: sulfur dioxide

Sulfur dioxide ice is dominant on the Jovian moon Io.[29] Two sets of experiments on SO_2 ice films were performed. In the first set of experiments gaseous SO_2 was deposited onto a CaF_2 substrate precooled to 25 K at a rate of 2.8 μm h^{-1}, until an ice film with a thickness of 0.30 μm had been prepared. This film was then annealed by raising the temperature of the ice to 80 K. To compare the effects of annealing to deposition temperature an ice film was prepared by depositing gaseous SO_2 onto the clean substrate at 80 K. In the second experimental set VUV photoabsorption spectra were

Table 5 Positions of vibrational bands (in eV) in pure solid (20 K) and gaseous (room temperature) N_2 spectrum

	$a^1\Pi_g \leftarrow \tilde{X}^1\Sigma_g^+$		$w^1\Delta_u \leftarrow \tilde{X}^1\Sigma_g^+$
ν'	Solid	Gas	Solid
0	8.51	8.54	8.84
1	8.72	8.74	9.02
2	8.93	8.95	9.21
3	9.12	9.15	9.40
4	9.32	9.34	9.58
5	9.52	9.54	9.76
6	9.70	9.73	9.94
7	9.89	9.91	10.11
8	10.07	10.10	10.44
9	10.25	10.27	10.28
10	10.42	10.444	10.62
			10.77

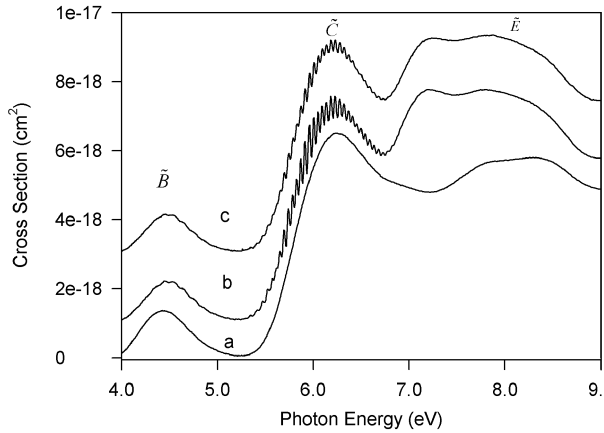

Fig. 8 Spectra of 'fast deposited' SO_2 (a) at 25 K, (b) at 80 K and (c) the sample deposited at 25 K subsequently annealed to 80 K.

recorded of SO_2 ice films grown at *a slower rate* of 0.21 μm h^{-1}, once again to a thickness of 0.30 μm and at a temperature of 25 K.

The VUV photoabsorption spectrum of solid SO_2 condensed at a rate of 2.8 μm h^{-1} onto the CaF_2 substrate (precooled to 25 K) [so called 'fast deposition'] is shown in Fig. 8a. Fig. 8b shows SO_2 deposited at 80 K. Fig. 8c shows SO_2 deposited at 25 K then annealed to 80 K. The 'slow deposition' of SO_2 deposited on the precooled substrate at 25 K at a rate of 0.21 μm h^{-1} is shown in Fig. 9.

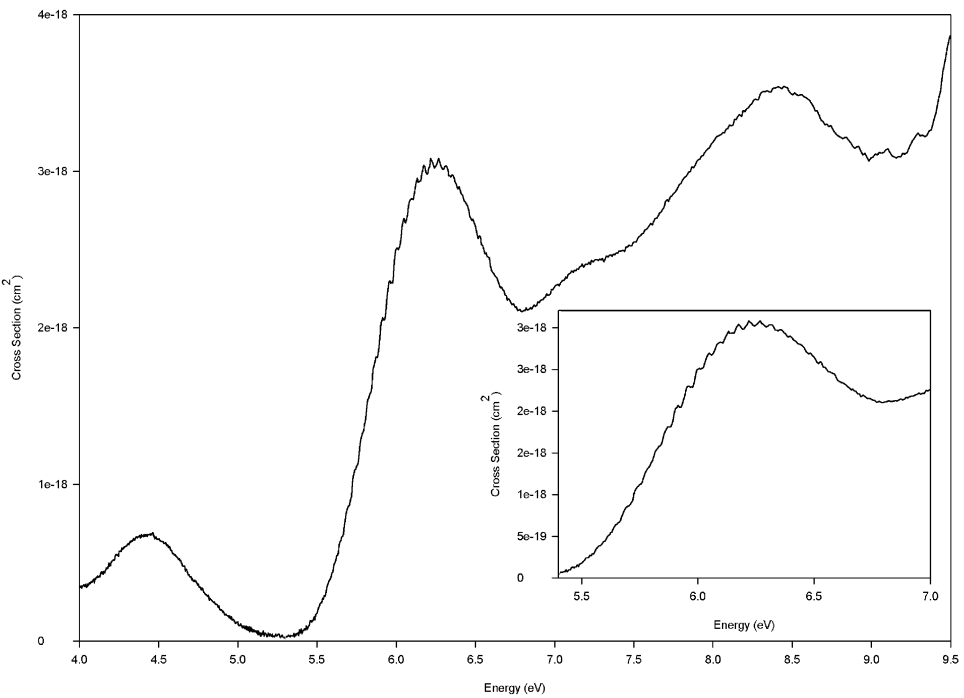

Fig. 9 Spectra of 'slow deposited' SO_2 at 25 K at a rate of 0.21 μm h^{-1}.

These spectra may be conveniently divided into three distinct regions: a broad continuum from 4 to 5.25 eV which is identified in the gas phase as the $\tilde{B}^1B_2 \leftarrow \tilde{X}^1A_1$ transition; a second band from 5.25 eV to 7 eV with a maximum at 6.28 eV which may be identified as corresponding to the $\tilde{C}^1B_2 \leftarrow \tilde{X}^1A_1$ transition in the gas phase; and a third region above 6.8 eV corresponding to the gas phase $\tilde{E}$ band as defined by Hertzberg.[30]

In contrast to the gas phase none of the electronic bands observed under conditons of fast deposition (Fig. 8a) show evidence of any vibrational structure. Fig. 8b and 8c show that there are no significant differences between a sample deposited at 80 K and one deposited at 25 K and then annealed to 80 K. Both spectra show vibrational structure in the lowest band structures between 4 and 7 eV and a new spectral feature showing an increased photoabsorption cross section in this region with respect to the non-annealed sample appears in the form of a broad peak at $\sim$7.2 eV.

From this data we can infer that our initial rapid deposition of SO_2 at 25 K is most likely to form a glassy, amorphous structure, as the rapid deposition and low temperatures will not allow the incident sulfur dioxide molecule time or mobility to convert to the more stable crystalline form. This is evident from the lack of vibrational structure on the electronic bands. In an amorphous solid there is no long range order but some short range order may still exist. The statistical distribution of the molecular environments of such a disordered solid can explain the broadening out and loss of vibrational structure. Upon heating, the additional input of energy should allow the ice to rearrange and form an ordered crystalline structure which, as it is more thermodynamically stable, is retained upon further cooling. This crystalline form of SO_2 ice allows the vibrational structure to propagate. In the crystalline form of ice we have a greater coupling between the molecules. Such coupling can increase the intensity of infrared features (and thus we assume their UV counterparts) by propagating a particular vibration through the crystal lattice.

Fig. 7 shows the VUV spectrum of a SO_2 ice deposited on the precooled substrate at 25 K at a rate of 0.21 μm h^{-1} ['slow deposition']. Unlike the spectrum recorded with the faster deposition rate (2.8 μm h^{-1}) shown in Fig. 8, vibrational structure is now clearly visible in the B and C bands of SO_2 ice. Additionally there is a small shoulder that suggests the presence of the 7.2 eV crystalline feature. This feature is attributed to Davydov splitting and is a clear marker of the crystalline morphology.

This suggests that with our slow deposition rates we are forming pockets of crystalline material on our substrate, as a slow deposition rate allows a greater probability of rearrangement to crystalline form. This has significant consequences for astrochemistry. In the interstellar medium it is likely that deposition timescales for individual molecules on interstellar dust grains are far greater than we can recreate in laboratory conditions. Hence this could suggest that any ice present in interstellar space could exhibit a structure similar to that observed during our longer deposition times, *i.e.* the characteristics of a more crystalline formation or that astrochemical ices are likely to be a mixture of crystalline and amorphous ices. Our recent data on ammonia illustrate this very well.

Case study 6: ammonia

Ammonia is believed to be an important interstellar nitrogen bearing molecule.[31] It is also a constituent of many planetary surfaces in our Solar System, including Pluto's satellite Charon,[32] and the Kuiper belt object Quaoar.[33] It therefore exists in a wide range of environments, spanning a wide temperature range and thermal history.

Two sets of experiments were carried out to investigate the photoabsorption spectrum of solid NH_3. In the first set of experiments NH_3 samples were deposited onto a precooled MgF_2 substrate at 25 K to a thickness of 0.24 μm and then annealed to higher temperatures. In the second set of experiments the same thickness of NH_3 was deposited at different temperatures above 50 K and once again annealed to higher temperatures to check for thermodynamic stability.

The spectrum of pure solid NH_3, between 5.5 and 9.9 eV deposited at 25 K shows a broad, smooth band peaking at 7.0 eV lacking all vibrational structure in comparison with the gas phase. This first absorption band is due to the $\tilde{A}^1A_2'' \leftarrow \tilde{X}^1A_1'$ molecular transition of NH_3, shifted to higher energy in the solid by 0.5 eV (15 nm), but with the shape and the intensity of the band appearing to trace the outline of the vibrational minima in the gas phase (Fig. 10). This blueshift is less than that observed in water and is probably due to weaker hydrogen bonding between the molecules. When the sample deposited at 25 K was annealed to higher temperatures (Fig. 11a,b) a

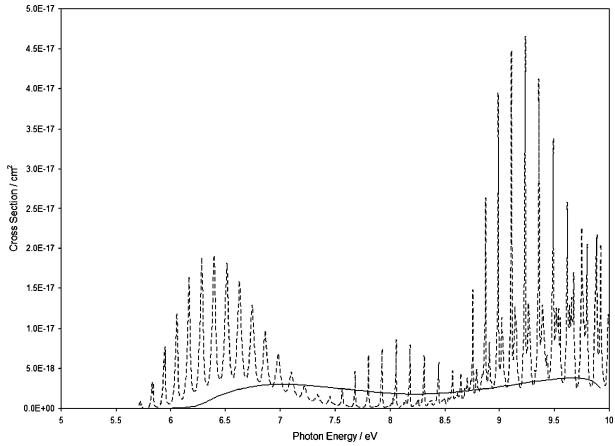

Fig. 10 VUV spectrum of solid ammonia deposited at 25 K (solid line) compared with the gas phase spectrum at room temperature (dashed line).

further 0.33 eV (8 nm) blueshift of the $\tilde{A} \leftarrow \tilde{X}$ band was observed in samples annealed to 70 K and above. Further annealing had no effect on the spectrum until the sample began to desorb from the surface between 110 and 125 K.

In the second experiment samples were deposited at different temperatures between 25 and 125 K. Above 65 K a dramatic change in the spectra was observed (Fig. 11c–e), with each spectrum looking very different but reproducible at each temperature. All spectra deposited above 65 K exhibit a relatively sharp feature at 6.39 eV (194 nm), the intensity of which decreases with increased deposition temperature.

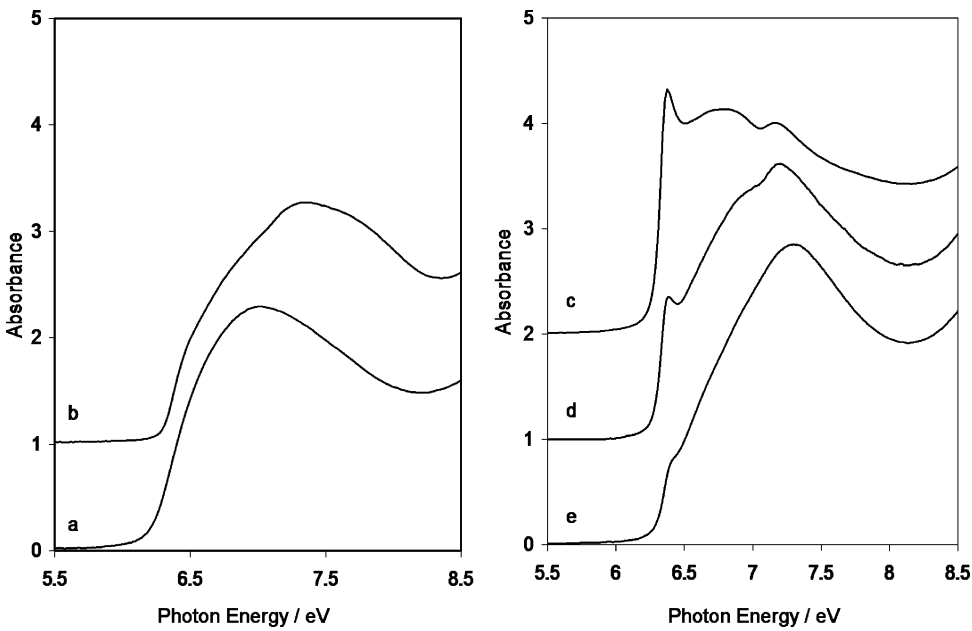

Fig. 11 Spectra of solid ammonia deposited at 25 K (a) and annealed to 75 K (b) (left) and solid ammonia deposited at (c) 75 K, (d) 85 K and (e) 95 K (right).

Like water, ammonia forms hydrogen bonds in the solid phase. In its crystalline cubic form the ammonia molecule donates and accepts six hydrogen bonds,[34] with the lone pair of electrons on the nitrogen atom shared between three hydrogen atoms, thus forming weaker hydrogen bonds than those found in crystalline water. This hydrogen bonding is believed to be responsible for the blue shift in the spectrum from the gas to the solid phase.[35] The further shift as the sample is annealed above 70 K is indicative of higher degree or more ordered hydrogen bonding as would be expected if the solid changes phase from a disordered to an ordered structure. The blueshift may be related to the fact that the electrons that are involved in the $\tilde{A}^1A_2'' \leftarrow \tilde{X}^1A_1'$ molecular transition also participate in the hydrogen bonding. A distortion of the non-bonding orbital is expected as hydrogen bonds are formed. Furthermore, during the transition $\tilde{A} \leftarrow \tilde{X}$ the molecule undergoes a dramatic change of geometry from a pyramidal to a planar symmetry. This change in geometry is likely to be perturbed in the solid phase due to intermolecular interactions.

The appearance of the relatively sharp feature at 6.39 eV (194 nm) at higher temperatures (>65 K) suggests that it is linked to the structure of the solid rather than a single molecular transition, and has been assigned to a Wannier exciton transition in the crystal.[16]

In the excited state of a free NH_3 molecule an electron is promoted to an extended atomic-like Rydberg orbital. In the solid these orbitals are greatly perturbed by surrounding molecules. The Rydberg orbitals in an ordered solid may have conduction band properties. In a molecular crystal with a large dielectric constant, promotion of an electron from a valence to a conduction band and the subsequent electron–hole pairing results in a Wannier exciton.

The structure of solid ammonia deposited above 65 K is thermodynamically stable and cannot be formed by annealing samples deposited at lower temperatures. One possible explanation for the origin of the exciton transition may be related to the formation of *crystallites* in the solid ammonia film; that is regions of crystallization within an amorphous ice. This is evident in Fig. 12 where different thicknesses of ammonia were deposited under the same conditions display different spectra. The prominence of the 'exciton' peak in thicker samples reflects a greater number of crystallites and hence the larger number of grain boundaries. The spectrum of the thin (0.03 μm) sample (Fig. 12a), on the other hand, is comparable to the spectrum of an amorphous sample. This indicates that, either there are no crystallites established or that they are not complete. It is expected that the size, shape and density of crystallites may affect the intensity of the exciton transition. It is to be noted that we observed little difference in the spectra of samples deposited at different rates other than a slight sharpening of the 194 nm band.

The properties and distribution of crystallites in the solid are governed by deposition conditions, particularly temperature. Based on this analysis it is possible to relate the temperature profile of solid ammonia to its structure:

(i) Samples *deposited below 50 K* are amorphous. This is a thermodynamically unstable structure that reorders upon annealing.

(ii) When *annealed above 65 K* the solid crystallises forming a thermodynamically stable structure. Steric effects prevent the formation of a complete ordered cubic structure.

(iii) *Deposited between 65 and 85 K*, all spectra of solid ammonia exhibit an intense exciton peak, with the highest intensity observed at around 70–75 K. The structure is composed of crystallites.

(iv) In samples *deposited at temperatures higher than 95 K* the exciton peak diminishes with increasing temperature. Crystallites are few and probably large such that the sample is an ordered cubic crystal with a thermodynamically stable structure.

Crystallites, if proven to be the common form of ice, will pose severe problems for the experimental community as it appears that the crystal : amorphous ratio may vary from deposition to deposition and will be strongly influenced by thermal processing history of the ice. The chemical reaction rates, molecular formation pathways and thermal desorption characteristics of such complex ices will all be dependent upon an almost random formation pattern making it difficult (impossible?) to produce mutually consistent sets of data in any one laboratory, yet alone across several laboratories. A similar phenomenon may occur in the formation of so-called clathrates (ice within which gases are trapped) which could play a key role in star and planet formation.

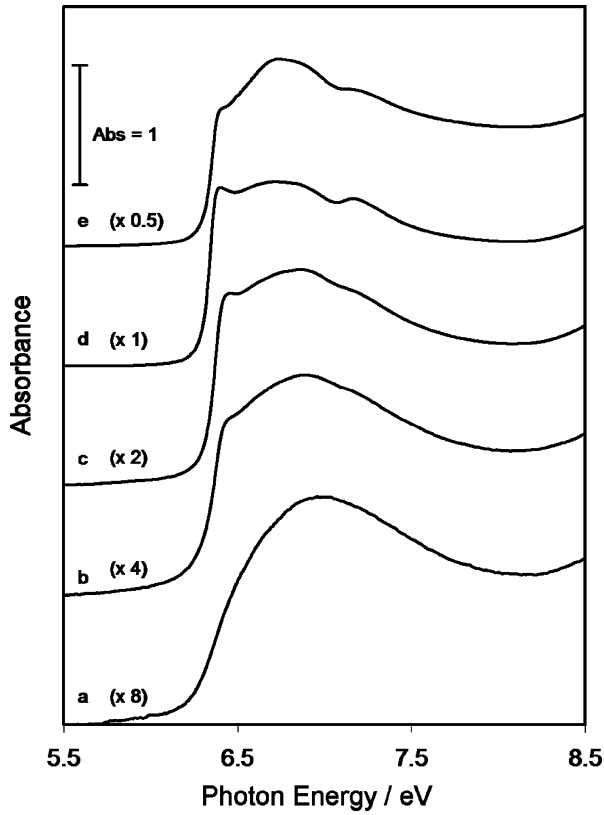

Fig. 12 Solid ammonia at 65 K deposited to different thicknesses: (a) 0.03 μm, (b) 0.06 μm, (c) 0.12 μm, (d) 0.24 μm and (e) 0.48 μm.

Conclusions and future studies

The present data combined with comparable data from IR studies shows that spectral analysis of ices is a useful tool for identifying the morphology of the ice under astronomical conditions. However such experiments are also revealing that the morphology of such ices is very sensitive to the preparation conditions of the ice *e.g.* fast or slow deposition and even the angle of incident molecular beam.[12] The morphology will also be strongly dependent upon the history of the ice arising from its inherent processing. Thus the heterogeneous phase chemistry on the ice surfaces in the universe will be hard to reproduce in the laboratory and there may be significant differences in the results recorded by different experimental groups arising from the methodology with which they both prepared and process their samples. This in turn will lead (has led?) to a bewildering set of seemingly conflicting experimental data with which observational astronomers and astrochemical modellers must contend. None of the data are 'wrong' *per se*; each may be valid within their own range of experimental parameters. But how might these be reconciled with those conditions in the ISM or on a particular planetary surface? We conclude this paper with some comments suitable for discussion at the Faraday meeting.

(i) Experimentally it is vital that different experiments are calibrated against one another such that the morphology of the ices used are compatible. A spectroscopic analysis of the nascent ice provides such a means both in the IR and UV. However this in turn requires a data base of ice spectra to be assembled similar to the large database of gas phase photo-absorption cross sections assembled by the atmospheric community. Such data must be recorded at different temperatures, deposition times and *for different substrates* since the latter may also influence the net morphology of the ice. The observation of clear spectral signatures directly comparable to a unique ice

morphology (*e.g.* observation of an exciton feature) would be the most useful calibrants. The formation of crystallites (and their gas containing counterpart clathrates), if they are common astrochemical objects, provide the ultimate experimental challenge since the inherent random nature of their formation ensures that no identical two samples can be formed even in the same apparatus. Thus the heterogeneous chemistry will be a statistical ensemble arising from the different physical structures.

(ii) The mimic of 'realistic' astrochemical conditions within the laboratory environment must be addressed. For example the data on SO_2 reveal that the ice morphology is dependent upon the deposition time. Laboratory time scales must necessarily be orders of magnitude less than astronomical time scales, how does this affect the physics and chemistry? For example in processing the ice with photon, electron or ion beams the incident laboratory flux is much larger than anything in space compressing the cosmic fluxes on the ice from 10^4 to 10^3 years into typically an hour in the laboratory. Within space therefore only single collisions are usually possible and there is time between events for the system to 'equilibrate' while in the laboratory several events may occur simultaneously within the ice sample.

(iii) To date most studies of astrochemical ices have used large bulk ice samples extending over substrates of several mm^2 whereas in the ISM the chemistry occurs on the surface of dust grains only a few microns in size. How is the physics and chemistry influenced by the surface area to volume ratio? Is the morphology on these grains compatible with that is a larger ice film? To explore this we have recently developed an ultrasonic trap (Fig. 13) within which we can suspend ice covered dust particles and hence study their spectral characteristics and coalescence properties. Such experiments may provide a means to test how the chemistry and physical characteristics of grains compares with the traditional bulk ice experiments.

However the development of new observational tools (*e.g.* the Spitzer space telescope, the VLO) and results from ongoing planetary missions (Cassini Huygens and Mars Express) are providing us with an ever increasing amount of data that will allow us to refine our experiments and provide increasingly realistic simulations of ices in the ISM and on planetary surfaces. For example very recently the Spitzer Space telescope has provided the first clear detection of ice in planet forming discs. Using Spitzer's ultra sensitive IR capability and viewing the circumstellar disk CRBR 2422.8-

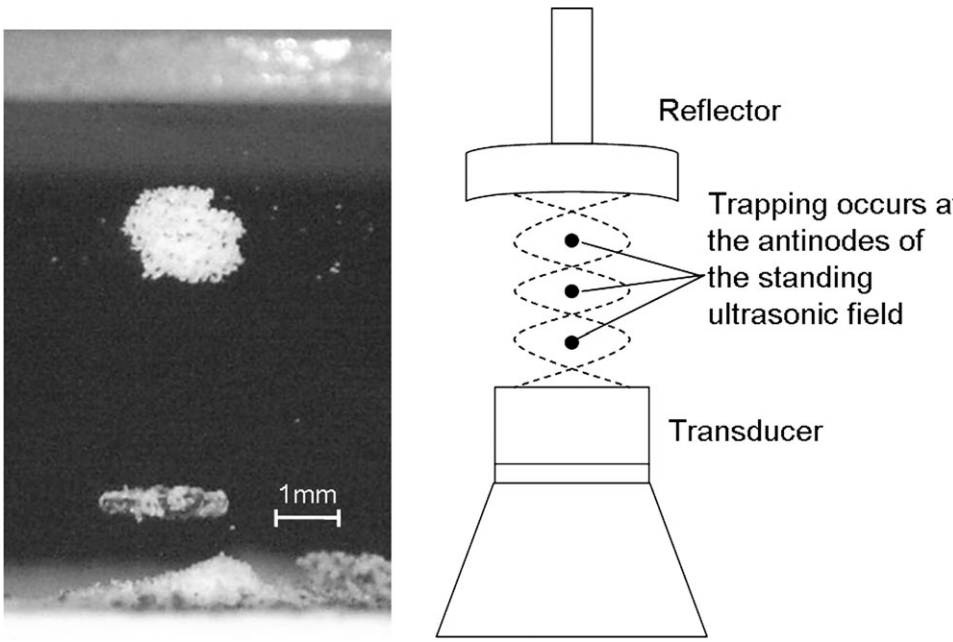

Fig. 13 Schematic diagram of an ultrasonic trap used to contain ice covered dust particles and study their spectral signature and coalescence properties (right). Soot and ice particles levitated within the trap (left).

3423 at a 20 degree angle, Pontoppidan *et al.*[36] have been able to distinguish ices in the inner planet forming part of the stellar disc from the larger outer envelope. The first results reveal ammonium ions as well as water and carbon dioxide ice providing a reference for laboratory experiments.[10]

Ultimately the combination of observation, modelling and laboratory studies will hopefully converge until we are satisfied that we understand the processes sufficiently to explain the observations and that must be the aim of astrochemistry in providing an explanation to the chemical evolution of the universe.

Acknowledgements

We wish to acknowledge receipt of support from the UK PPARC, EPSRC and NERC Funding councils as well as CLRC for access to the Daresbury Synchrotron facility and the EU for access to the Astrid Synchrotron facility at University of Aarhus, Denmark under the support given to the I3 project IA-SFS, contract number RII3-CT-2004-506008. AD acknowledges support of Postdoctoral Research Assistantship form PPARC; PDH a studentship from the EPSRC; MPD and BS support from the Open University. NJM is grateful for support from the EU Research Training Network Electron and Positron Induced Chemistry HPRN-C-2002-00179 and the ESF EIPAM programme.

References

1 J. C. Armstrong, T. N. Titus and H. H. Kieffer, *Icarus*, 2005, **174**, 360–372.
2 R. E. Milliken, J. F. Mustard, F. Poulet, J.-P. Bibring, Y. Langevin, B. Gondet, S. M. Pelkey and T. M. E. O. Team, *36th Annual Lunar and Planetary Science Conference*, Houston, Texas, 14–18 March 2005, *Lunar and Planetary Institute Contribution No. 1234*.
3 R. O. Kuzmin, E. V. Zabalueva, I. G. Mitrofanov, M. L. Litvak, W. V. Boynton and R. S. Saunders, *Sol. Syst. Res.*, 2004, **38**, 1–11.
4 J. A. Stansberry, D. J. Pisano and R. V. Yelle, *Planet. Space Sci.*, 1996, **44**, 945–955.
5 M. H. Carr, M. J. S. Belton, C. R. Chapman, M. E. Davies, P. Geissler, R. Greenberg, A. S. McEwen, B. R. Tufts, R. Greeley, R. Sullivan, J. W. Head, R. T. Pappalardo, K. P. Klaasen, T. V. Johnson, J. Kaufman, D. Senske, J. Moore, G. Neukum, G. Schubert, J. A. Burns, P. Thomas and J. Veverka, *Nature*, 1998, **391**, 363.
6 K. S. Noll, T. L. Roush, D. P. Cruikshank, R. E. Johnson and Y. J. Pendleton, *Nature*, 1997, **388**, 45–47.
7 K. S. Noll, R. E. Johnson, A. L. Lane, D. L. Domingue and H. A. Weaver, *Science*, 1996, **273**, 341.
8 D. Jewitt, *Annu. Rev. Earth Planet. Sci.*, 1999, **27**, 287–312.
9 A. W. Blain, I. Smail, R. J. Ivison and J.-P. Kneib, *Mon. Not. R. Astron. Soc.*, 1999, **302**, 632–648.
10 H. Wang, R. C. Bell, M. J. Iedema, A. A. Tsekouras and J. P. Cowin, *Astrophys. J.*, 2005, **620**, 1027–1032.
11 M. S. Westley, G. A. Baratta and R. A. Baragiola, *J. Chem. Phys.*, 1998, **108**, 3321–3326.
12 Z. Dohnálek, G. A. Kimmel, P. Ayotte, R. S. Smith and B. D. Kay, *J. Chem. Phys.*, 2003, **118**, 364–372.
13 M. P. Collings, J. W. Dever, H. J. Fraser, M. R. S. McCoustra and D. A. Williams, *Astrophys. J.*, 2003, **583**, 1058–1062.
14 R. Mota, R. Parafita, A. Giuliani, M.-J. Hubin-Franskin, J. M. C. Lourenco, G. Garcia, S. V. Hoffmann, N. J. Mason, P. A. Ribeiro, M. Raposo and P. Limao-Vieira, *Chem. Phys. Lett.*, 2005, **416**, 152–159.
15 D. S. McClure, *Electronic Spectra of Molecules and Ions in Crystals*, Academic Press, London, 1959.
16 M. B. Robin, *Higher Excited States of Polyatomic Molecules*, Academic Press, Inc., London, 1974.
17 S. R. Federman, D. L. Lambert, Y. Sheffer, J. A. Cardelli, B.-G. Andersson, E. F. van Dishoeck and J. Zsargoacute, *Astrophys. J.*, 2003, **591**, 986–999.
18 E. F. van Dishoeck and J. H. Black, *Astrophys. J.*, 1988, **334**, 771–802.
19 L. W. Beegle, J. M. Ajello, G. K. James, D. Dziczek and M. Alvarez, *Astron. Astrophys.*, 1999, **347**, 375–390.
20 M. E. Palumbo and G. Strazzulla, *Astron. Astrophys.*, 1993, **269**, 568–580.
21 S. A. Sandford, L. J. Allamandola, A. G. G. M. Tielens and G. J. Valero, *Astrophys. J.*, 1988, **329**, 498–510.
22 M. Brith and O. Schnepp, *Mol. Phys.*, 1965, **9**, 473.
23 M. C. Deschamps, M. Michaud and L. Sanche, *J. Chem. Phys.*, 2003, **119**, 9628–9632.
24 K. M. Monahan and W. C. Walker, *J. Chem. Phys.*, 1974, **61**, 3886–3889.
25 K. Yoshino, J. R. Esmond, Y. Sun, W. H. Parkinson, K. Ito and T. Matsiu, *J. Quant. Spectrosc. Radiat. Transfer*, 1996, **55**, 53–60.
26 P. Ehrenfreund and E. F. van Dishoeck, *Adv. Space Res.*, 1998, **21**, 15–20.
27 S. A. Sandford, M. P. Bernstein, L. J. Allamandola, D. Goorvitch and T. C. V. S. Teixeira, *Astrophys. J.*, 2001, **548**, 836–851.
28 E. Boursey, V. Chandrasekharan, P. Gürtler, E. E. Koch, P. Kunsch and V. Saile, *Phys. Rev. Lett.*, 1978, **41**, 1516–1519.

29 S. A. Sandford and L. J. Allamandola, *Icarus*, 1993, **106**, 478–488.
30 G. Herzberg, *Molecular Spectra and Molecular Structure III. Electronic Spectra and Electronic Structure of Polyatomic Molecules*, Van Nostrand Reinhold Company Ltd, New York, 1966.
31 R. Terzieva and E. Herbst, *Astrophys. J.*, 1998, **501**, 207.
32 M. E. Brown and a. W. M. Calvin, *Science*, 2000, **287**, 107–109.
33 D. C. Jewitt and J. Luu, *Nature*, 2004, **432**, 731–733.
34 I. Olovsson and D. H. Templeton, *Acta Crystallogr.*, 1959, **12**, 832–836.
35 K. Dressler and O. Schnepp, *J. Chem. Phys.*, 1960, **33**, 270–274.
36 K. M. Pontoppidan, C. P. Dullemond, E. F. van Dishoeck, G. A. Blake, A. C. A. Boogert, N. J. Evans, J. E. Kessler-Silacci and F. Lahuis, *Astrophys. J.*, 2005, **622**, 463–481.
37 E. L. Gibb, D. C. B. Whittet, W. A. Schutte, A. C. A. Boogert, J. E. Chiar, P. Ehrenfreund, P. A. Gerakines, J. V. Keane, A. G. G. M. Tielens, E. F. van Dishoeck and O. Kerkhof, *Astrophys. J.*, 2000, **536**, 347–356.